International Journal of Nanomedicine

Dovepress
Taylor & Francis Group

Open Access Full Text Article

ORIGINAL RESEARCH

Lung Tissue Extracellular Vesicles-Mediated Delivery of miR-128-3p as a Novel Mechanism of Acute Lung Inflammation

Wei Deng[1–3], Xiaoping Zhu[3], Hang Li[4], Ping Hu[1,2], Kejian Qian[1,2], Fen Liu[1,2]

[1]Department of Critical Medicine, The First Affiliated Hospital of Nanchang University, Nanchang, People's Republic of China; [2]Medical Innovation Center, First Affiliated Hospital of Nanchang University, Nanchang, People's Republic of China; [3]Department of Anesthesiology, The First Affiliated Hospital of Nanchang University, Nanchang, People's Republic of China; [4]Department of Dermatology, The First Affiliated Hospital of Nanchang University, Nanchang, People's Republic of China

Correspondence: Fen Liu, Email liufen9934@163.com

Background: Emerging evidence links macrophage overactivation to sepsis-associated acute lung injury (ALI), yet the role of lung tissue-derived extracellular vesicles (Ti-EVs) in this process remains unclear. This study combines transcriptomic profiling and functional validation to reveal how Lung Ti-EVs mediate macrophage polarization through miRNA-dependent NLRP3 inflammasome activation.

Methods: We established a sepsis mouse model, extracted and characterized lung tissue-derived EVs, performed high-throughput transcriptome sequencing and bioinformatics analysis. Intratracheal administration of these EVs to wild-type C57BL/6 mice revealed their effects on pulmonary inflammation, macrophage polarization, and proliferation. In vitro co-culture experiments with Raw264.7 macrophages further validated these findings and explored underlying mechanisms.

Results: We identified extracellular vesicles (EVs) enriched in lung tissues from septic ALI mice, selectively carrying miRNAs including miR-128-3p. In vivo administration of these EVs exacerbated pulmonary inflammation by expanding M1 macrophage populations, while in vitro experiments demonstrated EV-mediated miR-128-3p delivery to macrophages stimulated TNF-α and IL-6 production. Mechanistically, miR-128-3p promoted macrophage proliferation and inflammatory responses by targeting Rab20.

Keywords: lung tissue extracellular vesicles, sepsis, acute lung inflammation, miR-128-3p, macrophages

Introduction

Sepsis is a life-threatening clinical syndrome characterized by high incidence and mortality rates.[1,2] The lungs are the primary target organ during sepsis, with approximately 25% to 50% of sepsis patients developing acute lung injury (ALI) or progressing to acute respiratory distress syndrome.[3] Of particular concern is the higher mortality rate associated with ALI caused by sepsis compared to other risk factors.[4] Despite continuous optimization of clinical treatment methods for sepsis-induced ALI, the mortality rate remains unacceptably high at 40%.[5] Therefore, there is an urgent need to explore safe and effective strategies for treating ALI.

Inflammation is a fundamental biological process that maintains homeostasis. However, excessive inflammatory responses can result in tissue damage. The inflammatory response in acute lung injury (ALI) involves various target cells and effector cells,[6] with macrophages playing a pivotal role. Macrophages serve as crucial effectors and regulators of the inflammatory cascade triggered by ALI, participating in pathogen clearance and promoting adaptive immune responses.[7] The polarization of macrophages, namely classical activation (M1) and alternative activation (M2), plays a key role in fulfilling these functions.[8] M1 macrophages are recognized for their pro-inflammatory properties, critically involved in phagocytosis and secretion of pro-inflammatory cytokines; whereas M2 macrophages primarily contribute to inflammation regulation and tissue repair.[9,10] Excessive production of M1 macrophages following sepsis-induced ALI can exacerbate lung inflammation and alveolar injury, thereby worsening the severity of sepsis-induced ALI.[11] Conversely, the generation of M2 macrophages facilitates alveolar repair

Received: 4 December 2024
Accepted: 5 April 2025
Published: 15 April 2025

and regeneration, thus aiding recovery from sepsis-induced ALI.[12] Therefore, targeting the polarization of macrophages during sepsis-induced ALI is considered a potential therapeutic approach.

Extracellular Vesicles (EVs) are extracellular vesicles ranging in diameter from 30 to 150 nm, enclosed by a double-layered membrane and containing molecular components derived from their source cells, including immune-suppressive and immune-stimulating proteins, chemokines, cytokines, cell receptors, lipids, microRNAs (miRNA), long non-coding RNAs (LncRNA), and messenger RNAs (mRNA).[13–15] Recent investigations have elucidated their roles in the regulation of inflammation and confirmed their involvement in various diseases through the modulation of macrophage polarization.[16] Extensive research has demonstrated the significance of non-coding RNAs particularly miRNAs in acute lung injury.[14] EVs possess the ability to transfer specific molecules such as miRNAs into target cells for regulating cellular functions and participating in disease mechanisms.[17] In a mouse model of sepsis-induced lung injury, EVs containing miRNA play a regulatory role in macrophages and mediate the systemic response to acute lung injury.[18,19] However, most studies have focused on isolating EVs from cell culture systems and body fluids.[20,21] Compared to EVs derived from these sources, tissue-derived extracellular vesicles (Ti-EVs), which are directly isolated from the interstitial space surrounding various cell types, can provide more comprehensive information that accurately reflects subtle changes within cells and tissue microenvironments with higher tissue specificity.[22] Bowen Li et al discovered that under inflammatory conditions, lung Ti-EVs can aggregate in the bone marrow and enhance neutrophil recruitment.[23] Cecilia Lässer et al demonstrated that Ti-EVs derived from lung tissues can be isolated in mice, and their proteomics undergo changes during allergen-induced airway inflammation, potentially contributing to the pathogenesis of type 2-driven eosinophilic asthma.[24] Yang et al demonstrated that M2 macrophage-derived extracellular vesicles (EVs) effectively inhibit alveolar macrophage pyroptosis both in vitro and in vivo via a miR-709-mediated mechanism, suppressing the excessive release of cytokines such as IL-6, TNF-α, and IL-1β, thereby attenuating acute lung injury.[12] In a separate study, Chen et al identified that EV-let-7a-5p modulates M2-like macrophage activation in inflammatory microenvironments, significantly reducing macrophage infiltration and collagen deposition while upregulating IL-10 expression, which markedly improves pulmonary function.[25] However, limited knowledge exists regarding the involvement and mechanisms of action of EVs derived from lung tissue in acute lung injury. This study presents novel findings demonstrating that EVs originating from lung tissue exacerbate sepsis-induced acute lung injury, thereby suggesting that early inhibition of these lung-derived EVs may hold promise as a potential therapeutic strategy. Specifically, we have identified the miRNA profile within EVs derived from lung tissue during sepsis-induced acute lung injury and elucidated the Ti-EVs-miR-128-3p-M1 polarization axis within the lungs under this pathological condition.

Materials and Methods

Mice

C57BL/6J mice (male, aged 6–8 weeks) were obtained from Zhejiang Weitonglihua Experimental Animal Co., Ltd. in China. The mice were maintained under controlled conditions of temperature (23–24°C), humidity (55±5%), and a 12-hour light-dark cycle. All animal experiments received approval from the Animal Ethics Committee of the First Affiliated Hospital of Nanchang University (Ethics Approval Number: CDYFY-IACUC-202302QR051) and were conducted in compliance with the National Institutes of Health (NIH) guidelines for the care and use of laboratory animals, as well as relevant regulations outlined in China's Regulations on the Administration of Experimental Animals. Random grouping was achieved using computer-generated numbers.

Cell Culture

The mouse macrophages were obtained from Shanghai Fuxiang Biotechnology Co., Ltd. (Shanghai, China). The cells were maintained in high-glucose DMEM supplemented with 10% FBS, streptomycin at a concentration of 50 mg/mL, and penicillin at a concentration of 50 U/mL. They were incubated in a humidified environment at 37°C with 5% CO2. Fresh medium was replaced daily, and when the cell density reached approximately 80% to 90%, the cells were subcultured.

Mouse Model of Cecal Ligation and Puncture (CLP)-Induced ALI

Following the methodology outlined in previous literature, a sepsis mouse model was established through CLP surgery.[26] Prior to the CLP procedure, mice were subjected to an 8-hour fasting period and a 4-hour water restriction. Subsequently, anesthesia was induced via intraperitoneal injection of 0.3% pentobarbital sodium at a dosage of 30 mg/kg (Rui Tai, China). The limbs of the mice were secured on the surgical table, after which abdominal fur was shaved and depilatory cream applied; iodine solution was utilized for disinfection. A midline incision measuring 1.0–2.0 cm below the diaphragm was performed to expose the cecum. Following ligation of approximately 50% of the cecal tip, an 18G needle was employed to puncture the ligated site twice in both directions, allowing for gentle extrusion of intestinal contents from the needle holes. The cecum was then carefully repositioned into the abdominal cavity, with closure achieved using a 4–0 suture for both muscle and skin incisions. Mice in the sham surgery group did not undergo cecal puncture or ligation; all other procedures mirrored those conducted on CLP group mice. Postoperatively, mice were placed on a heating pad to maintain normothermia and received resuscitation via subcutaneous injection of 1 mL pre-warmed saline (37°C).

Lung Histological Analysis

Lung tissues were removed and preserved in formalin for 24 hours to facilitate subsequent histological examination. The samples were then embedded in paraffin, sectioned at a thickness of 4 μm, and stained using hematoxylin and eosin.

Myeloperoxidase (MPO) Evaluation

MPO activity was assessed to measure the infiltration of inflammatory cells into lung tissues. Lung samples were homogenized in a reaction buffer at a ratio of 1:9 (w/v), and MPO activity was evaluated using a commercial test kit from WuHan Elabscience Biotechnology Co., Ltd, China, following the manufacturer's guidelines.

RNA Extraction and qPCR Analysis

Total RNA was isolated using TRIzol reagent (Invitrogen, USA). Reverse transcription PCR was carried out in a 20 μL reaction volume following the manufacturer's protocol. Subsequently, qPCR was performed with SYBR Green Master Mix on a StepOne Plus Real-Time PCR System (Applied Biosystems, USA). The relative expression levels of miRNAs or mRNAs were normalized using the $2^{-\Delta\Delta Ct}$ method, employing U6 small nuclear RNA (snRNA) or GAPDH as reference genes.

Isolation of EVs from Lung Tissue

To extract lung tissue-derived EVs, lung tissue from animals in both the CLP and sham groups was carefully cut into small pieces (approximately 2 × 2×2 mm) and stored at −80°C, following previously described methods[27] with slight modifications.[28] The tissue mixture was dissociated using the Miltenyi human tumor dissociation kit (Miltenyi Biotec, cat. no. 130–095-929). Enzymes H, R, and A were utilized according to the manufacturer's guidelines. A fresh mixture consisting of 2.2 mL RPMI medium, 100 μL enzyme H, 50 μL enzyme R, and 12.5 μL enzyme A was prepared just before use. Approximately 200 mg of tissue was briefly sliced on dry ice and then incubated in the dissociation solution at 37°C for about 10–15 minutes. The resulting suspension was filtered twice through a 70 μM filter to eliminate any remaining tissue fragments. Following a centrifugation step at 4°C for ten minutes at a speed of 300× g, the supernatant was transferred to a new tube and subjected to another centrifugation for ten minutes at a speed of 2000 × g under similar conditions. The cell-free supernatant was gradually passed through a filter with a pore size of 0.22 μm to remove cellular debris before being centrifuged again at an acceleration of 10,000 × g for thirty minutes at four degrees Celsius (Optima XPN-100 using Beckman ultra-clear tubes). The resultant suspension underwent ultracentrifugation at an acceleration of 150,000× g for two hours at four degrees Celsius to collect the pellet which was then resuspended in one milliliter PBS; Exosupur column chromatography purification followed (Echobiotech, China). Finally, fractions were concentrated down to two hundred microliters using Amicon® Ultra spin filters with a molecular weight cutoff of 100 kDa (Merck, Germany).

Transmission Electron Microscopy (TEM)

The lung tissue-derived EVs solution was applied to a copper mesh and incubated for one minute at room temperature. Subsequently, lung tissue-derived EVs were rinsed with sterile distilled water and stained with uranyl acetate solution for one minute. The sample was then dried under incandescent light for two minutes. Transmission electron microscopy (TEM; H-7650, Hitachi Ltd., Tokyo, Japan) was employed to visualize and capture images of the copper mesh.

Nanoparticle Tracking Analysis (NTA)

The ZetaView PMX 110 (Particle Metrix, Meerbusch, Germany), which is equipped with a 405 nm laser, was utilized to assess the size and concentration of particles in vesicle suspensions. Particle motion was analyzed using NTA software (ZetaView 8.02.28) based on a 60-second video recorded at 30 frames per second.

Western Blot Analysis

Protein concentrations were determined using the Bicinchoninic Acid (BCA) Protein Assay Kit (Bio-Rad, Hercules, CA, USA). Equal volumes of protein samples were subjected to sodium dodecyl sulfate polyacrylamide gel electrophoresis and subsequently transferred onto polyvinylidene difluoride (PVDF) membranes. The membranes were incubated with 5% non-fat milk for one hour at room temperature to block nonspecific binding, followed by an overnight incubation at 4°C with antibodies specific to CD63 (1:500 dilution, Santa Cruz Biotechnology, USA), CD9 (1:1000 dilution, Santa Cruz Biotechnology, USA), GM130 (1:1000 dilution, Santa Cruz Biotechnology, USA), TSG101 (1:1000 dilution, Santa Cruz Biotechnology, USA), NLRP3 (1:1000 dilution, dilution, Abcam, UK), Rab20 (1:1000 dilution, Abcam, UK), and β-actin (1:5000 dilution, Santa Cruz Biotechnology, USA). The following day, the membranes were rinsed and incubated with horseradish peroxidase (HRP)-conjugated secondary antibodies (1:1000, Cell Signaling Technology, USA). Detection of the blots was performed using enhanced chemiluminescence (Thermo Fisher Scientific, Bei Jing, China), and quantification was carried out with the Bio-Rad imaging system (USA). β-actin served as a loading control, and the relative intensity of the target protein was normalized to that of the control group.

RNA Isolation, Library Preparation, and RNA Sequencing

Lung tissue-derived EVs for RNA sequencing were isolated from both sham and CLP groups. Total RNA was extracted and purified from lung tissue EVs using the miRNeasy Serum/Plasma Advanced Kit (Qiagen, cat. No. 217204), in accordance with the manufacturer's guidelines. The concentration and purity of RNA were assessed utilizing the RNA Nano 6000 assay kit along with the Agilent Bioanalyzer 2100 System (Agilent Technologies, CA, USA). For library construction, 4.5 ng of RNA from each sample was used as input material with the SMARTer Stranded total RNA-Seq Kit V2 (Takara Bio USA, Inc). Index codes were subsequently incorporated into each sample's attribute sequences. In preparing small RNA libraries, a total of 3 ng of RNA per sample served as input material for generating the samples. The QIAseq miRNA library kit (Qiagen, Frederick, MD) facilitated sequencing library generation while index codes were added to their respective attribute sequences. Unique molecular indices in reverse transcription primers enabled quantification of miRNA expression during cDNA synthesis and PCR amplification processes. Finally, library quality assessment was performed using both the Agilent Bioanalyzer 2100 and qPCR methods. Clustering of index-coded samples on the acBot cluster generation system followed manufacturer's instructions using TruSeq PE Cluster Kitv3-cBot-HS (Illumina, San Diego, CA, USA). After clustering completion, sequencing preparations were conducted on the Illumina NovaSeq 6000 platform by EchoBiotech Co., Ltd., based in China.

miRNA Analysis

Bowtie software was employed to align the Clean Reads with the Silva, GtRNAdb, Rfam, and Repbase databases. Repeats and non-coding RNAs (ncRNAs), including ribosomal RNA (rRNA), transfer RNA (tRNA), small nuclear RNA (snRNA), and small nucleolar RNA (snoRNA), were removed from consideration. The remaining reads were used to identify and predict miRNAs by comparing them against known miRNAs sourced from miRbase and Genome (ftp://ftp.ensembl.org/pub/release-101/fasta/mus_musculus/dna). The expression matrix for the quantitative unique molecular

index count of miRNA was normalized to transcripts per million and calculated as relative logarithmic expression using the EdgeR package.

Immunofluorescent Staining

The cells or excised tissues were fixed in formalin, treated with 0.1% Triton X-100 for permeabilization, and blocked using 10% BSA. Samples were incubated overnight at 4°C with primary antibodies, followed by a one-hour incubation at 25°C with fluorescently labeled secondary antibodies. Nuclei were stained with DAPI for ten minutes to visualize them. Fluorescent microscopy (Leica, Wetzlar, Germany) was employed to capture six images from each animal. The following antibodies were utilized: anti-CD68 (28,058-1-AP, dilution of 1:100; Proteintech), anti-iNOS (18985-1-AP, dilution of 1:100; Proteintech), anti-Arg-1 (16,001-1-AP, dilution of 1:100; Proteintech), anti-CD80 (66,406-1-lg, dilution of 1:100; Proteintech) and anti-EDU (Ribo Biotech Co., Ltd., China).

Bioluminescence Imaging

We employed the Sigma PKH67 Green Fluorescent Labeling Kit (MINI67) to label EVs, adhering to the previously established protocol.[29] Subsequently, we co-cultured these labeled EVs with macrophages; after a designated incubation period, we stained the macrophages with DAPI and examined them using a fluorescence microscope. Concurrently, in accordance with the manufacturer's instructions, we labeled EVs utilizing fluorescent lipophilic tracers DiR/DiI (5 μM, AAT Bioquest) and DAPI (10 μg/mL, Beyotime). Briefly, EVs were diluted in PBS prior to dye application. The labeling process was conducted at room temperature in darkness for 20 minutes and subsequently terminated by adding 0.1% BSA (Sigma Aldrich) in PBS. The EVs were then centrifuged at 110,000×g for 70 minutes to eliminate any residual free dye before being resuspended in PBS and transferred into recipient mice for bioluminescence imaging using the Xenogen IVIS imaging system.

Cell Transfection

Following the manufacturer's guidelines, the riboFECT^{TM} CP Reagent (Ribobio Technology Co., Ltd., Guangzhou, China) was utilized to transfect the specified small interfering RNA (siRNA) or negative controls (NCs) into macrophages. Cells were collected for subsequent analyses 12 hours post-transfection. agomir-NC, agomir-128-3p, antagomir-NC, antagomir-128-3p, minic-NC, minic-128-3p, Inhibitor-NC, Inhibitor-128-3p, siRNA and corresponding negative control siRNA (si-NC) were designed and synthesized by Ribobio Technology Co., Ltd. (Guangzhou, China).

Luciferase Assay

The 3'-UTR region of the Rab20 gene encompasses predicted binding sites for miR-128-3p and its mutants, which were subsequently cloned into a plasmid vector and transfected into HEK293 cells. In all transfection experiments, a firefly luciferase vector was co-transfected to assess transfection efficiency. All luciferase results were reported as relative luminescence units: the average observed firefly luciferase activity was normalized against the average activity recorded from the firefly luciferase vector.

Cell Proliferation Assays

Adhere to the guidelines provided in the EDU kit to conduct the EDU experiment. Incubate 4×10^3 to 1×10^5 cells in a culture medium supplemented with EDU (Ribobio Technology Co., Ltd., China) for a duration of 2 hours prior to performing immunostaining. Fluorescence images were captured using a fluorescence microscope (Zeiss, Germany).

Preparation of Engineered Lung Tissue EVs

Lung tissue EVs were mixed with a 20μM miR-128-3p agonist or inhibitor to achieve a total volume of 400μL, maintaining an approximate ratio of 400μg EVs per 1OD miRNA (5 nmol). The resulting mixture was transferred to a 0.4cm electroporation cuvette and placed on ice. Electroporation parameters were set at 400V for 15ms. Following electroporation, RNase was employed to eliminate any unloaded miRNA adhering to the exosomal surface (10μL RNase

at a concentration of 1 mg/mL incubated for 10 minutes to remove untransfected miRNA). Subsequently, ultracentrifugation was performed at 150,000×g for 2 hours. Finally, the sample was stored at −80°C for future use.

Statistical Analysis

Data analysis was performed using SPSS 26.0 software, and graphs were created using GraphPad Prism 8.3.0 software. For data that followed a normal distribution, the mean (standard deviation) was used. For comparisons between two groups, we used a *t*-test, and for comparisons between three groups, we used one-way analysis of variance. For data that did not follow a normal distribution, the median (interquartile range) was used, and comparisons between two groups were made using the Mann–Whitney *U*-test, and comparisons between three groups were made using the Kruskal–Wallis test. $P < 0.05$ was considered statistically significant.

Results

Activated Macrophages in the Lung Tissue of Mice with Acute Lung Injury

Initially, we employed HE staining to assess the successful establishment of the mouse sepsis-induced acute lung injury (ALI) model. Compared to the Sham group, lung tissue from the CLP group exhibited significant pathological alterations, including interstitial edema, alveolar hemorrhage, and infiltration of inflammatory cells (Figure 1A), confirming that a viable mouse sepsis-induced ALI model was established. We noted a marked increase in the expression levels of inflammatory factors IL-1β, IL-6, and TNF-α in the ALI-induced group following CLP when compared with the Sham group (Figure 1B). Myeloperoxidase (MPO) serves as a critical indicator of inflammatory cell accumulation; results indicated an elevated degree of lung inflammation in the CLP group relative to the Sham group (Figure 1C). Macrophages play a pivotal role in ALI's inflammatory response; thus, we utilized immunofluorescence to evaluate CD68 expression as a macrophage marker within lung tissue. Our findings revealed that fluorescence intensity for macrophages significantly increased in the CLP group compared to controls (Figure 1D). Subsequently, we analyzed markers indicative of activated macrophage phenotypes: iNOS (M1) and Arg1 (M2). Immunofluorescence data demonstrated an increase in fluorescence intensity for pro-inflammatory M1 macrophages within the CLP cohort while anti-inflammatory M2 macrophages displayed reduced fluorescence intensity (Figure 1E and F). Additionally, we observed an elevation in mRNA levels for specific M1 marker CD80 within the CLP group alongside decreased expression of M2-specific marker CD206—further corroborating our immunofluorescence findings (Figure 1G).

Isolation and Characterization of Lung Tissue-Derived EVs

Lung Ti-EVs were extracted separately from the lung tissues of both the Sham and CLP groups, and their ultrastructure was examined using transmission electron microscopy (TEM) (Figure 2A). TEM images revealed that these Ti-EVs exhibited a cup-like morphology. Additionally, we characterized the size distribution of lung tissue-derived Ti-EVs isolated from both groups utilizing a ZetaView nanoparticle tracking analyzer (Figure 2B). As illustrated in the figure, there was a significant increase in the concentration of lung tissue-derived Ti-EVs in the CLP group; however, no differences were observed in EV size. Furthermore, Western blot analysis confirmed that the markers CD9, CD63, and TSG101 in Ti-EVs derived from lung tissues of both the Sham and CLP groups were positively expressed.[15] These findings validate our successful extraction of lung tissue-derived Ti-EVs.

Ti-EVs Isolated from the Lung Tissues of Mice with Sepsis-Induced ALI Exacerbate ALI via M1 Macrophage Polarization

We injected lung Ti-EVs from sepsis ALI mice via tracheal administration to assess their role in inducing lung injury. In vivo imaging showed that these Ti-EVs accumulated in the lung tissue after injection (Figure 3A). Our findings suggest that lung Ti-EVs may contribute to ALI. To further investigate whether these EVs induce lung inflammation, we administered Ti-EVs from Sham and CLP mouse lungs into Sham-Exo and CLP-Exo groups, respectively. Histological analysis revealed significant pathological changes in the lungs of CLP-Exo mice compared to Sham-Exo, including interstitial edema, alveolar congestion, and inflammatory cell infiltration (Figure 3B). Additionally, we

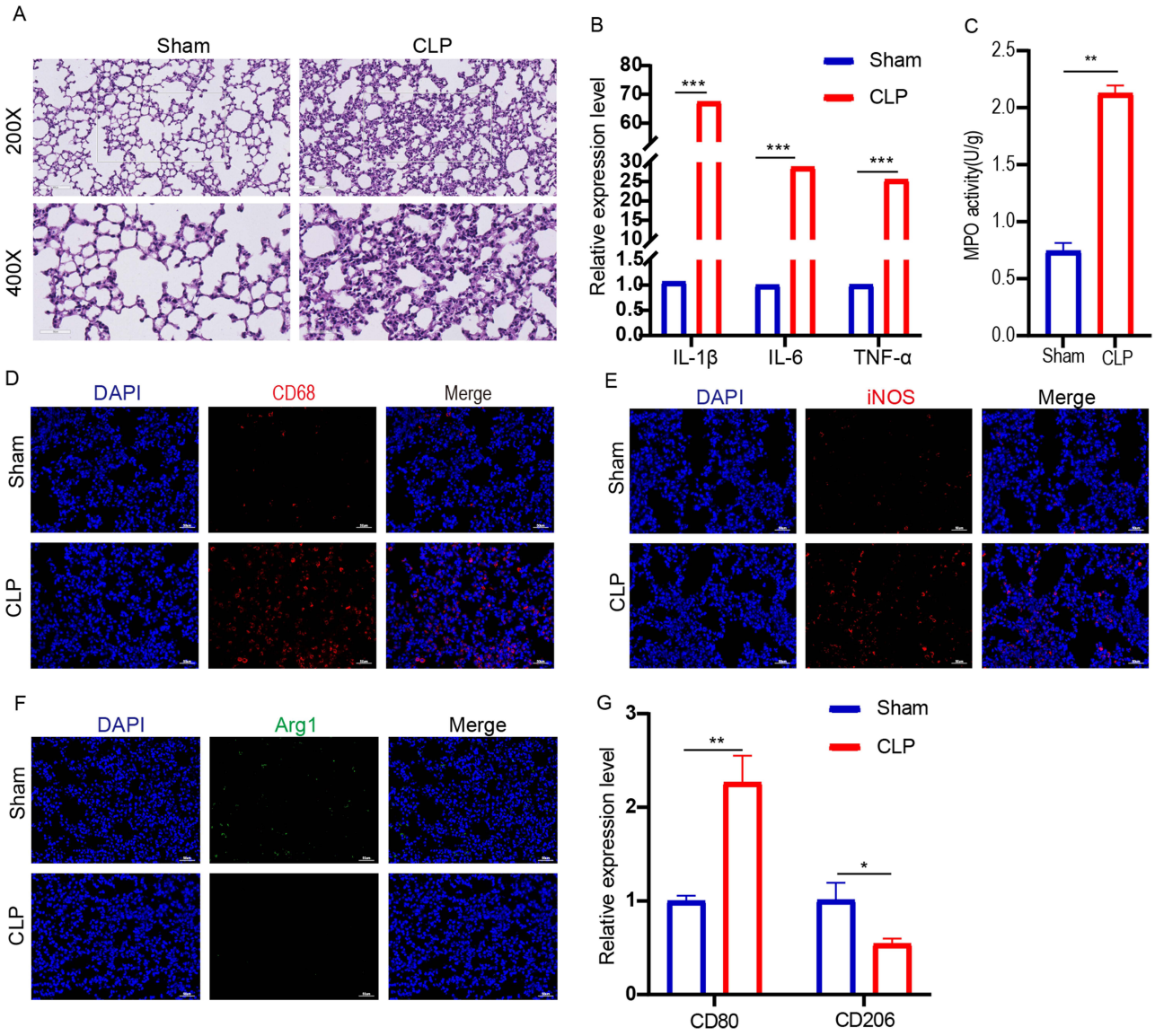

Figure 1 Macrophages in the lung tissues of ALI mice were activated. (**A**) Pathological analysis of lung tissues was conducted. Following the establishment of the CLP model for 24 hours, H&E staining was employed to evaluate the degree of lung inflammation (n=6), with images at 200x magnification corresponding to a scale of 100μm and those at 400x magnification corresponding to a scale of 50μm. (**B**) The expression levels of inflammatory factors IL-1β, IL-6, and TNF-α were quantified using qRT-PCR (n=6). (**C**) Infiltration of inflammatory cells within lung tissues was assessed by measuring MPO activity (n=6). (**D**) After sectioning, immunofluorescence intensity for CD68-positive macrophages in lung tissues was determined through anti-CD68 antibody staining (n=6), scale bar 50μm. (**E**) Immunofluorescence intensity for M1 macrophages in lung tissues was evaluated using iNOS as a marker (M1, red), scale bar 50μm. (**F**) Immunofluorescence intensity for M2 macrophages in lung tissues was assessed with Arg1 as a marker (M2, green), scale bar 50μm. (**G**) Expression levels of CD80 and CD206 were measured via qRT-PCR, utilizing GAPDH as an endogenous control (n=6). **P*<0.05, ***P*<0.01, ****P*<0.001.

measured pro-inflammatory cytokines IL-1β, IL-6, and TNF-α in the lung tissue; qRT-PCR results indicated elevated levels of these cytokines in the CLP-Exo group relative to Sham-Exo controls (Figure 3C). Macrophage polarization is crucial for damage response and repair during sepsis-induced ALI. Next, we used immunofluorescence staining to determine if pulmonary Ti-EVs enhance macrophage proliferation and modulate activation status in vivo. The results showed an increase in macrophage numbers within the CLP-Exo group compared with Sham-Exo (Figure 3D), along with increased M1 macrophage markers while M2 markers were reduced (Figure 3E and F). Furthermore, mRNA levels for CD80—a specific marker for M1 macrophages—were significantly higher (Figure 3G), whereas expression of M2 marker CD206 was lower. Finally, we quantified the expression level of miR-128-3p and observed that it was significantly elevated in the lung tissue of mice in the CLP-Exo group compared to other groups (Figure 3H).

https://doi.org/10.2147/IJN.S510241

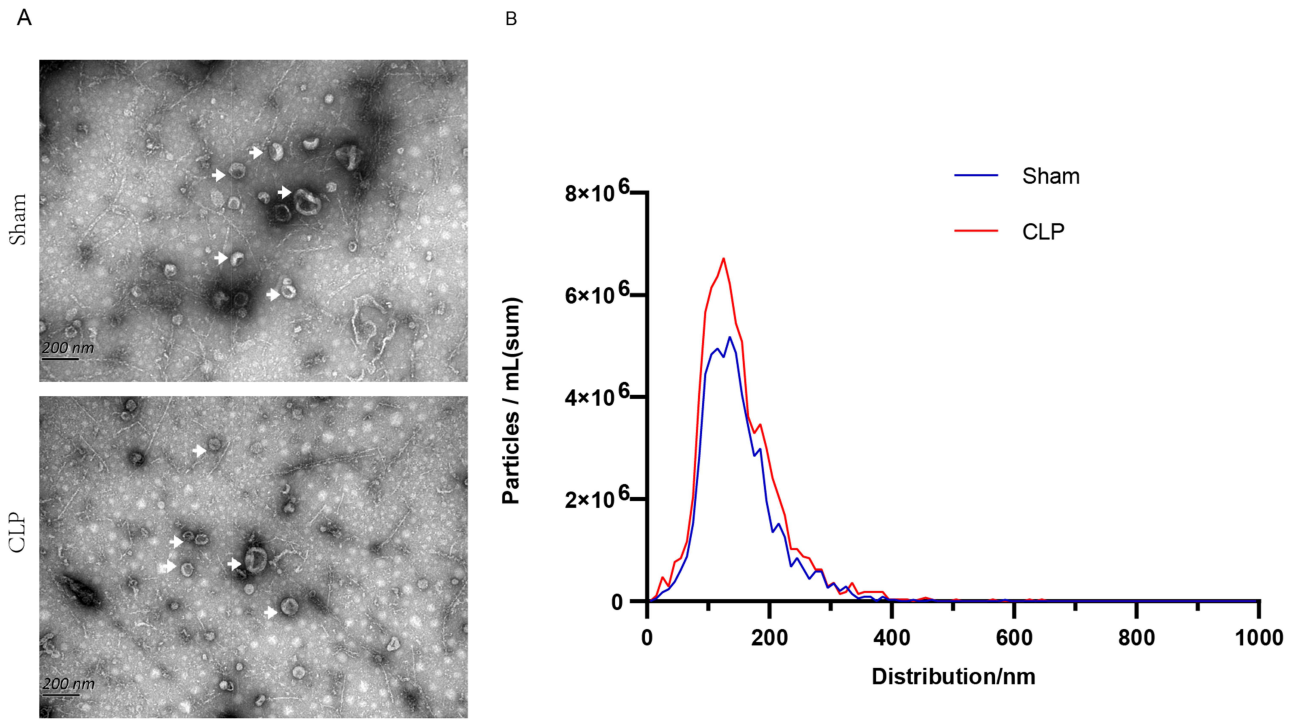

Figure 2 Isolation and characterization of lung Ti-EVs. (**A**) Transmission electron microscopy images depict lung Ti-EVs isolated from the lung tissues of mice in both the Sham and CLP groups, which were subjected to acute lung injury. The scale bar represents 200 nm, with white arrows in (**A**) indicating EV particles. (**B**) Nanoparticle tracking analysis (NTA) reveals the concentration and size distribution of lung Ti-EVs obtained from the Sham and CLP group mice (n=6).

Inhibition of Ti-EVs Production in the Lungs Mitigates ALI Induced by M1 Macrophage Polarization

We utilized GW4869, a well-characterized chemical inhibitor of EVs/exosome biogenesis, to examine the effects of inhibiting lung Ti-EVs on septic ALI.[30] Initially, DMSO or GW4869 (1 mg/kg) was administered through intraperitoneal injection into mice one hour prior to the experimental procedures. Subsequently, both Sham and CLP groups were established, and lung tissues were collected from each group 24 hours later. Histological analysis demonstrated that the pathological changes in the lung tissues of the CLP+GW4869 group were significantly less severe compared to those observed in the CLP+DMSO group (Figure 4A). Concurrently, we evaluated pro-inflammatory cytokines such as IL-1β, IL-6, and TNF-α within the lung tissues. Quantitative RT-PCR results indicated that levels of these pro-inflammatory factors were substantially lower in the CLP +GW4869 group relative to those in the CLP+DMSO group (Figure 4B). Additionally, we observed a reduction in macrophage numbers within the CLP+GW4869 cohort when compared with their counterparts in the CLP+DMSO group (Figure 4C), along with decreased fluorescence intensity for M1 macrophages and fewer markers indicative of M2 macrophages (Figure 4D and E). Furthermore, mRNA levels for CD80—a specific marker for M1 macrophages—were found to be diminished (Figure 4F), while expression levels of another M2 marker CD206 increased, thereby supporting our immunofluorescence findings. Finally, we assessed miR-128-3p expression levels and discovered that they were highest in lung tissues from mice subjected to CLP+DMSO treatment (Figure 4G). Macrophages were co-incubated with EVs isolated from lung tissue. qPCR was employed to assess the expression levels of the top 8 upregulated miRNAs in EVs derived from both Sham and CLP groups, as identified through miRNA sequencing. The results demonstrated that miR-128-3p exhibited the highest expression level in the EVs obtained from the CLP-Exo group (Figure 4H).

Lung Ti-EVs from Pneumonia-Associated Sepsis ALI Selectively Encapsulate miR-128-3p

Recent research has demonstrated that EVs play a crucial role in regulating the physiological functions of target cells through the delivery of microRNAs (miRNAs). Based on our previously published sequencing study, bioinformatics analysis revealed miRNAs with significantly upregulated expression levels, and quantitative RT-PCR was conducted to assess their differential

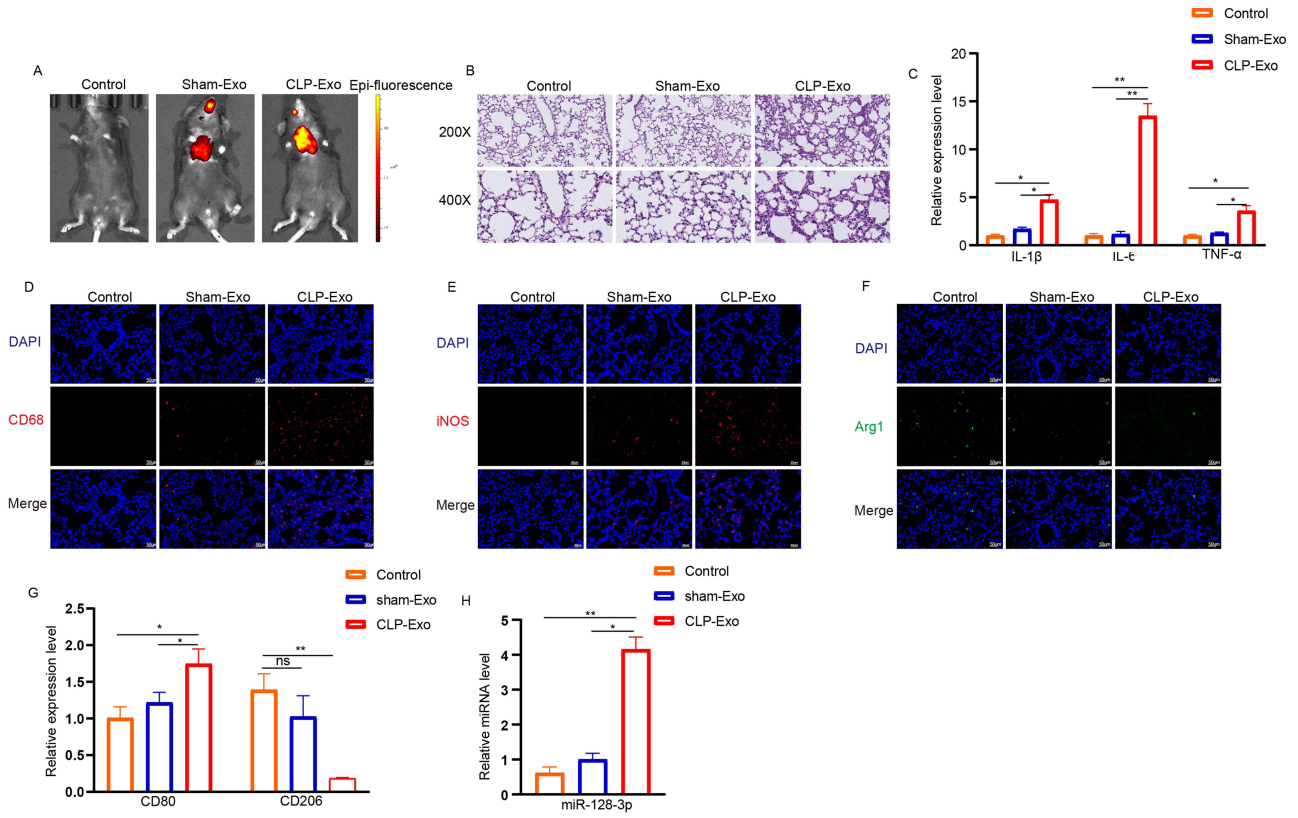

Figure 3 Injection of EVs derived from the lung tissue of ALI mice induces lung inflammation in recipient mice. (**A**) Fluorescent signals observed in the lungs following intratracheal injection of DiR-labeled EVs. (**B**) Pathological analysis of lung tissue was conducted after establishing the CLP model for 24 hours, with H&E staining used to evaluate the extent of lung inflammation (n=6). Images at 200x magnification correspond to a scale bar of 100μm, while those at 400x magnification correspond to a scale bar of 50μm. (**C**) qRT-PCR was employed to assess mRNA expression levels of inflammatory cytokines IL-1β, IL-6, and TNF-α in lung tissue. (**D**) Following sectioning, immunofluorescence intensity for macrophage marker CD68 in lung tissue was determined using anti-CD68 antibody staining (n=6; CD68 shown in red). (**E**) Immunofluorescence intensity for M1 macrophages within lung tissue is presented (n=6), with iNOS as an M1 marker shown in red. (**F**) Immunofluorescence intensity for M2 macrophages within lung tissue is depicted (n=6), with Arg1 as an M2 marker shown in green. (**G**) Expression levels of CD80 and CD206 were quantified via qRT-PCR, utilizing GAPDH as an endogenous control (n=6). (**H**) miR-128-3p expression levels were also assessed by qRT-PCR. **P*<0.05, ***P*<0.01, ns *P*>0.05.

expression in lung Ti-EVs.[15] Notably, miR-128-3p exhibited the highest expression level in CLP-Exo compared to Sham-Exo, indicating that EVs derived from lung tissue of ALI mice may selectively encapsulate miR-128-3p (Figure 4H).

Lung Ti-EVs Carrying miR-128-3p Enhance Macrophage Proliferation and Inflammation in vivo

To investigate the role of miR-128-3p in lung Ti-EVs on the phenotypic transformation of macrophages during septic ALI, agomir, a miR-128-3p agonist, or agomir NC as a control was introduced into lung Ti-EVs via electroporation. The resulting engineered exosomes, either agomir-miR-128-3p or agomir-NC, were subsequently administered intratracheally to mice. Results indicated that treatment with engineered exosomes containing agomir-miR-128-3p led to exacerbation of histological lesions (Figure 5A), increased expression levels of pro-inflammatory cytokines IL-1β, IL-6, and TNF-α (Figure 5B), as well as an elevation in both the number of lung macrophages and M1 macrophage activation (Figure 5C and D). Moreover, mRNA levels of the specific M1 marker CD80 were significantly elevated while those of another M2 marker CD206 were reduced (Figure 5E). This finding was further corroborated by additional data showing increased mRNA levels for CD80 alongside decreased expression for CD206 (Figure 5F), reinforcing immunofluorescence results. Collectively, these findings suggest that engineered exosomes carrying agomir-miR-128-3p exacerbate sepsis-induced ALI through enhanced activation of M1 macrophages.

https://doi.org/10.2147/IJN.S510241

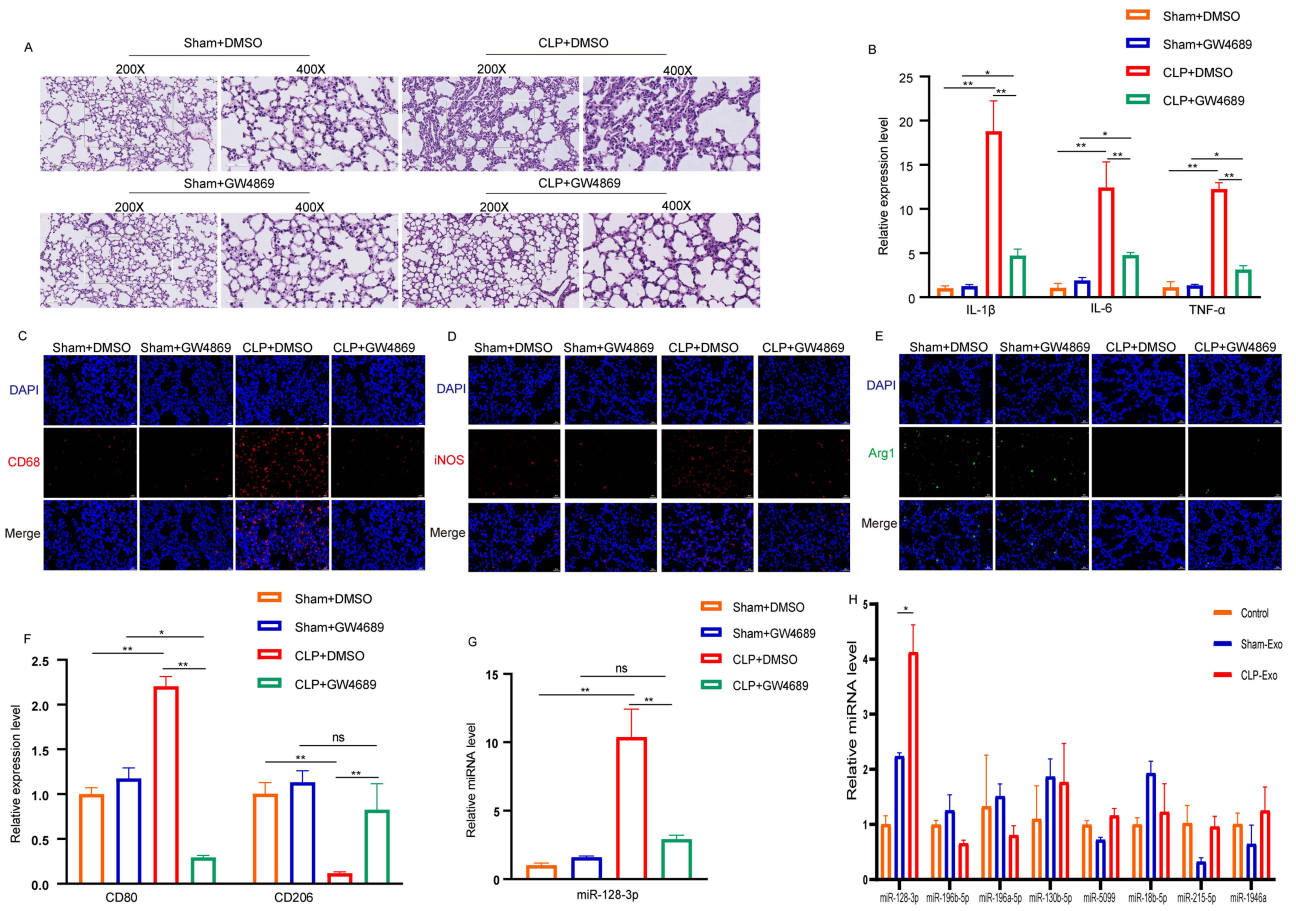

Figure 4 GW4869 mitigates sepsis-induced ALI and attenuates pulmonary inflammatory responses. (**A**) A pathological analysis of lung tissue was performed. Following the establishment of the CLP model for 24 hours, the degree of lung inflammation was evaluated using H&E staining (n=6). Images at 200x magnification correspond to a scale bar of 100μm, while those at 400x magnification correspond to a scale bar of 50μm. (**B**) Quantitative RT-PCR was utilized to quantify the expression levels of inflammatory cytokine mRNA in lung tissue, including IL-1β, IL-6, and TNF-α. (**C**) After sectioning, immunofluorescence intensity for CD68-positive macrophages in lung tissue was assessed through anti-CD68 antibody staining (n=6; CD68 shown in red), scale bar 50μm. (**D**) The immunofluorescence intensity for M1-type macrophages within lung tissue is presented (n=6), with iNOS as an M1 marker depicted in red, scale bar 50μm. (**E**) The immunofluorescence intensity for M2-type macrophages in lung tissue is illustrated (n=6), with Arg1 serving as an M2 marker shown in green, scale bar 50μm. (**F**) Expression levels of CD80 and CD206 were quantified via qRT-PCR, employing GAPDH as an endogenous control (n=6). (**G**) miR-128-3p expression levels were also measured by qRT-PCR (n=6). (**H**) Quantitative RT-PCR was employed to assess the expression levels of exosomal miR-128-3p in Raw264.7 macrophages following treatment with Sham-Exo and CLP-Exo (n=6). **P*<0.05, ***P*<0.01, ns *P*>0.05.

Lung Ti-EVs Carrying miR-128-3p Enhance Proliferation and Inflammation in vitro Macrophages

To investigate the involvement of lung Ti-EVs miR-128-3p in the phenotypic transformation of macrophages during the vitro development of septic ALI, we labeled lung Ti-EVs with PKH67 and co-cultured them with macrophages in culture medium for 6 hours. We observed that macrophages were capable of internalizing these lung Ti-EVs in vitro (Figure 6A). Furthermore, upon stimulation with CLP-Exo, levels of miR-128-3p significantly increased (Figure 6B), indicating that miR-128-3p from lung Ti-EVs derived from ALI mice can be transferred to macrophages. To assess macrophage proliferation, we employed the EDU method. The results demonstrated that CLP-Exo enhanced macrophage proliferation compared to Sham-Exo (Figure 6C). Immunofluorescence analysis confirmed a significant increase in fluorescence intensity for iNOS and CD80 on CLP-Exo-treated macrophages, suggesting that CLP-Exo-induced proliferation is associated with an increase in M1 macrophages (Figure 6D and E). Additionally, we evaluated the inflammatory effects of lung Ti-EVs on macrophages. Compared to cells stimulated by Sham-Exo, those treated with CLP-Exo exhibited significantly elevated levels of pro-inflammatory cytokines IL-6, IL-1β, and TNF-α (Figure 6F). NLRP3 is a cytosolic immune factor responsive to cellular stress signals and regulates downstream inflammatory cytokines involved in inflammation processes. Our findings revealed that NLRP3 expression was higher in CLP-exposed cells than in those

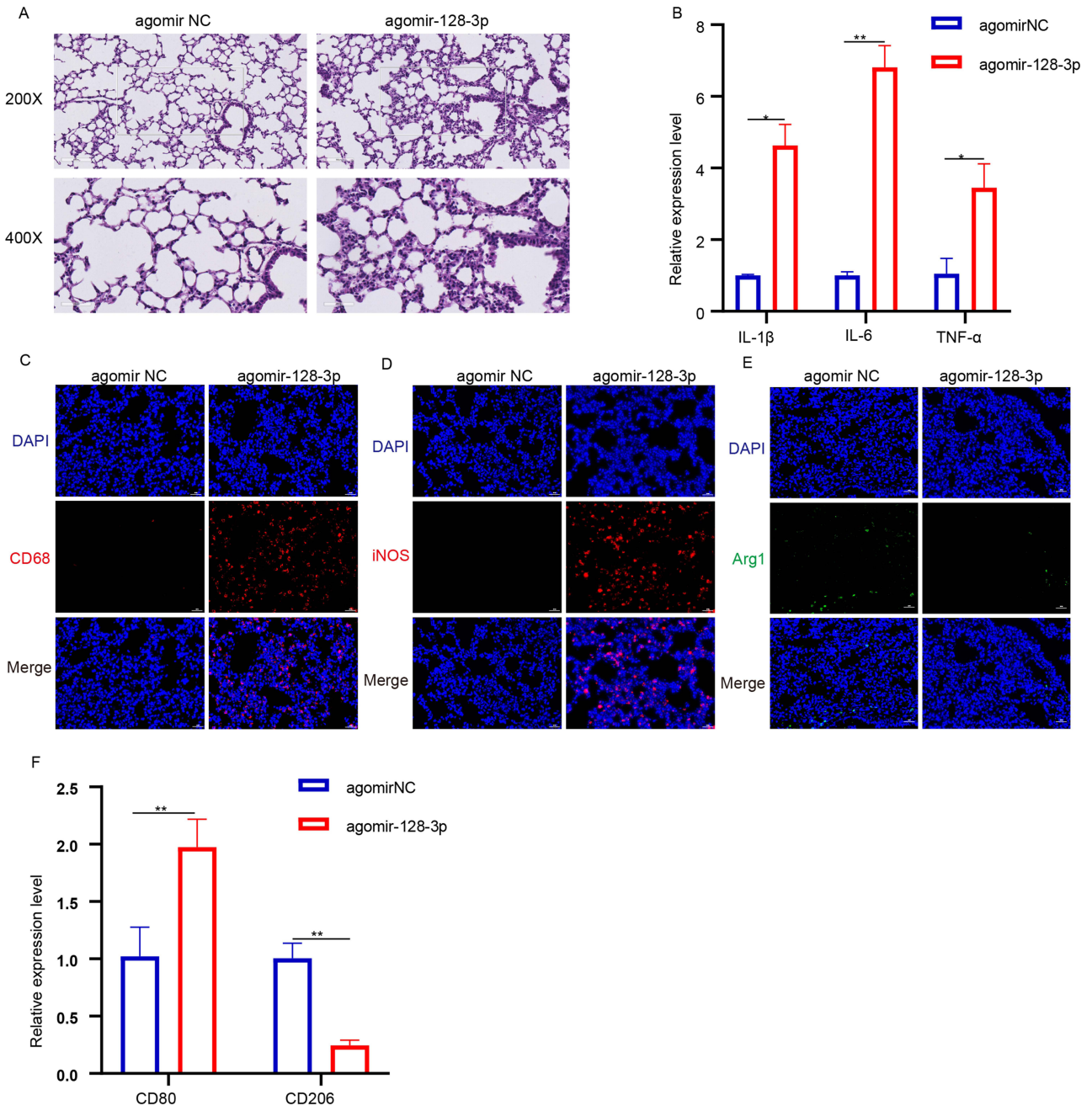

Figure 5 Lung Ti-EVs enhance the proliferation and inflammation of macrophages in vivo. (**A**) Pathological analysis of lung tissue was conducted, with the degree of inflammation assessed via H&E staining following a 24-hour establishment of the CLP model (n=6). Images at 200x magnification correspond to a scale bar of 100μm, while those at 400x magnification correspond to a scale bar of 50μm. (**B**) Quantitative RT-PCR was employed to measure mRNA expression levels of inflammatory cytokines (IL-1β, IL-6, TNF-α) in lung tissue. (**C**) Immunofluorescence staining was performed to evaluate the fluorescence intensity of CD68-positive macrophages in lung sections (n=6), scale bar 50μm. (**D**) The immune fluorescence intensity for M1-type macrophages in lung tissue was assessed using iNOS as a marker (M1, red), scale bar 50μm. (**E**) Similarly, immunofluorescence staining evaluated M2-type macrophage fluorescence intensity using Arg1 as a marker (M2, green), scale bar 50μm. (**F**) qRT-PCR analysis quantified the expression levels of CD80 and CD206, with GAPDH serving as an endogenous control (n=6). **P*<0.05, ***P*<0.01, ns *P*>0.05.

exposed to Sham Exosomes while Rab20 protein levels were reduced (Figure 6G). To further elucidate the role of miR-128-3p-containing lung Ti-EVs in promoting both proliferation and inflammation within macrophages, we co-cultured these cells with engineered exosomes minic-miR-128-3p. It was found that, compared with the exosomes from the minic-miR-128-3p NC group, the engineered exosomes containing minic-miR-128-3p significantly enhanced cell proliferation and inflammatory response (Figure 6H and I).

https://doi.org/10.2147/IJN.S510241

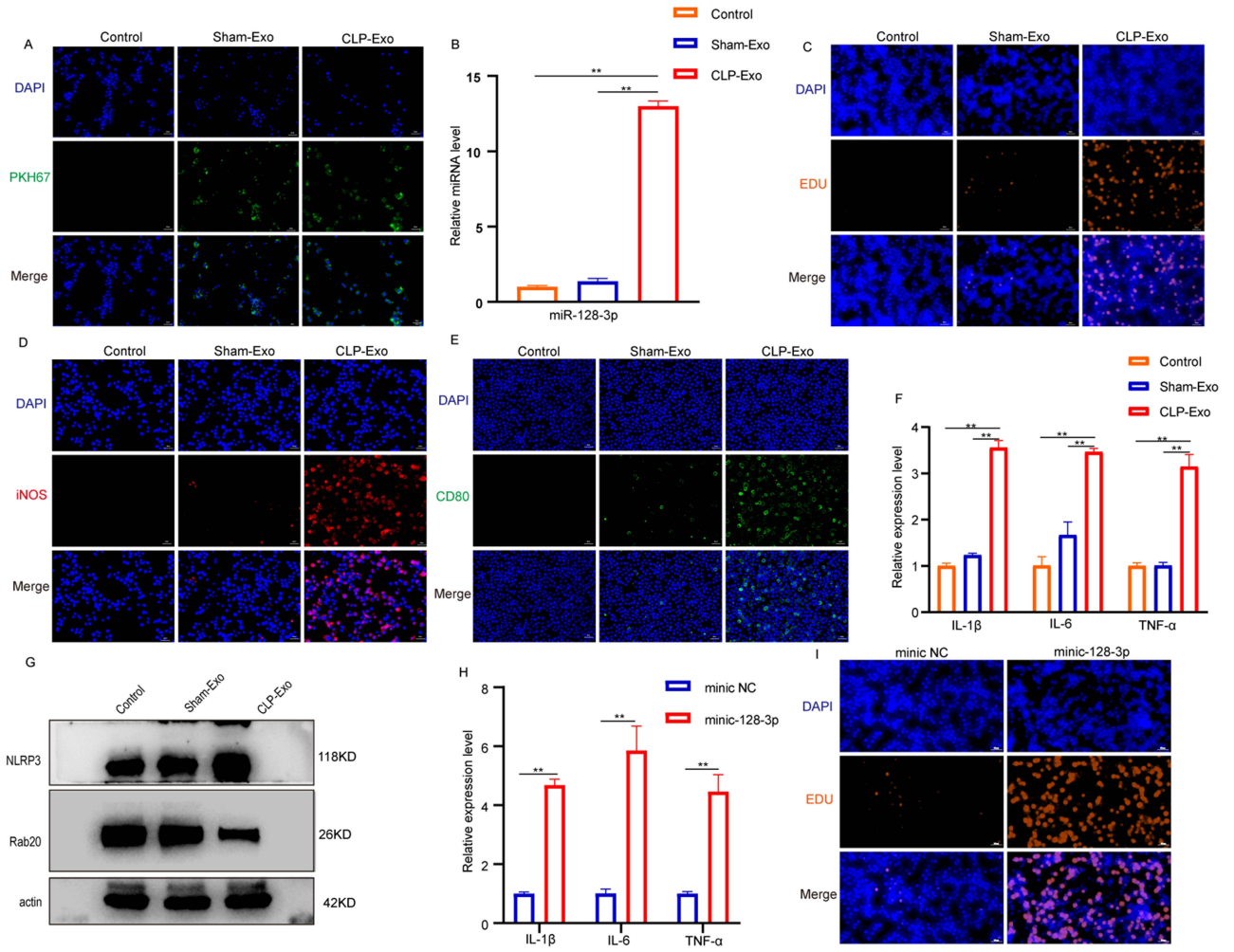

Figure 6 Lung Ti-EVs enhance macrophage proliferation and inflammation in vitro. (**A**) PKH67-labeled EVs (green) were co-cultured with macrophages for specified durations, and the uptake of exosomes by macrophages was observed using fluorescence microscopy (n=6), scale bar 50μm. (**B**) Ti-EVs from sham-operated and CLP-operated lung tissues were co-incubated with macrophages (Sham-Exo or CLP-Exo), followed by detection of miR-128-3p expression via qRT-PCR, utilizing U6 as an endogenous control (n=6). (**C**) The impact of lung tissue exosomes on macrophage proliferation was assessed using the EDU method (n=6), scale bar 50μm. (**D**) Immunofluorescence intensity of M1 macrophages was measured, highlighting iNOS expression (M1, red; n=6), scale bar 50μm. (**E**) Immunofluorescence intensity for CD80 in M1 macrophages is presented as well (M1, green; n=6), scale bar 50μm. (**F**) Expression levels of miR-128-3p and CD206 were quantified through qRT-PCR, with GAPDH serving as an endogenous control (n=6). Additionally, inflammatory cytokine mRNA expressions IL-1β, IL-6, and TNF-α were evaluated in lung tissue post incubation with Sham-Exo or CLP-Exo via qRT-PCR analysis (n=6). (**G**) Western blotting was employed to assess Rab20 and NLRP3 protein levels in lung tissue following incubation with Sham-Exo or CLP-Exo; β-actin served as an internal control. Finally, (**H**) the expression levels of inflammatory cytokine mRNAs IL-1β, IL-6, and TNF-α in lung tissue after incubation with minic-miR-128-3p versus minic-miR-128-3p NC were determined using qRT-PCR. (I) The effect of lung Ti-EVs on macrophage proliferation was further evaluated through the EDU method after exposure to engineered exosomes, scale bar 50μm. $^{**}P<0.01$, ns $P>0.05$.

miR-128-3p Enhances Macrophage Proliferation and Inflammation Through the Targeting of Rab20

Subsequently, we investigated the potential targets of miR-128-3p implicated in macrophage proliferation and inflammation to elucidate the molecular mechanisms by which miR-128-3p influences these processes. Bioinformatics analysis revealed that the 3' UTR of Rab20 mRNA harbors a complementary binding site for the seed region of miR-128-3p, which is conserved across species (Figure 7A). To further confirm whether Rab20 directly interacts with miR-128-3p, we performed a luciferase reporter assay. The results indicated that minic-miR-128-3p significantly reduced luciferase activity from the wild-type 3' UTR of Rab20 but had no effect on the luciferase activity from its mutant counterpart (Figure 7B). When engineered exosomes containing minic-miR-128-3p or minic-miR-128-3p NC were co-incubated with macrophages, overexpression of miR-128-3p inhibited Rab20 expression while increasing NLRP3 levels (Figure 7C).

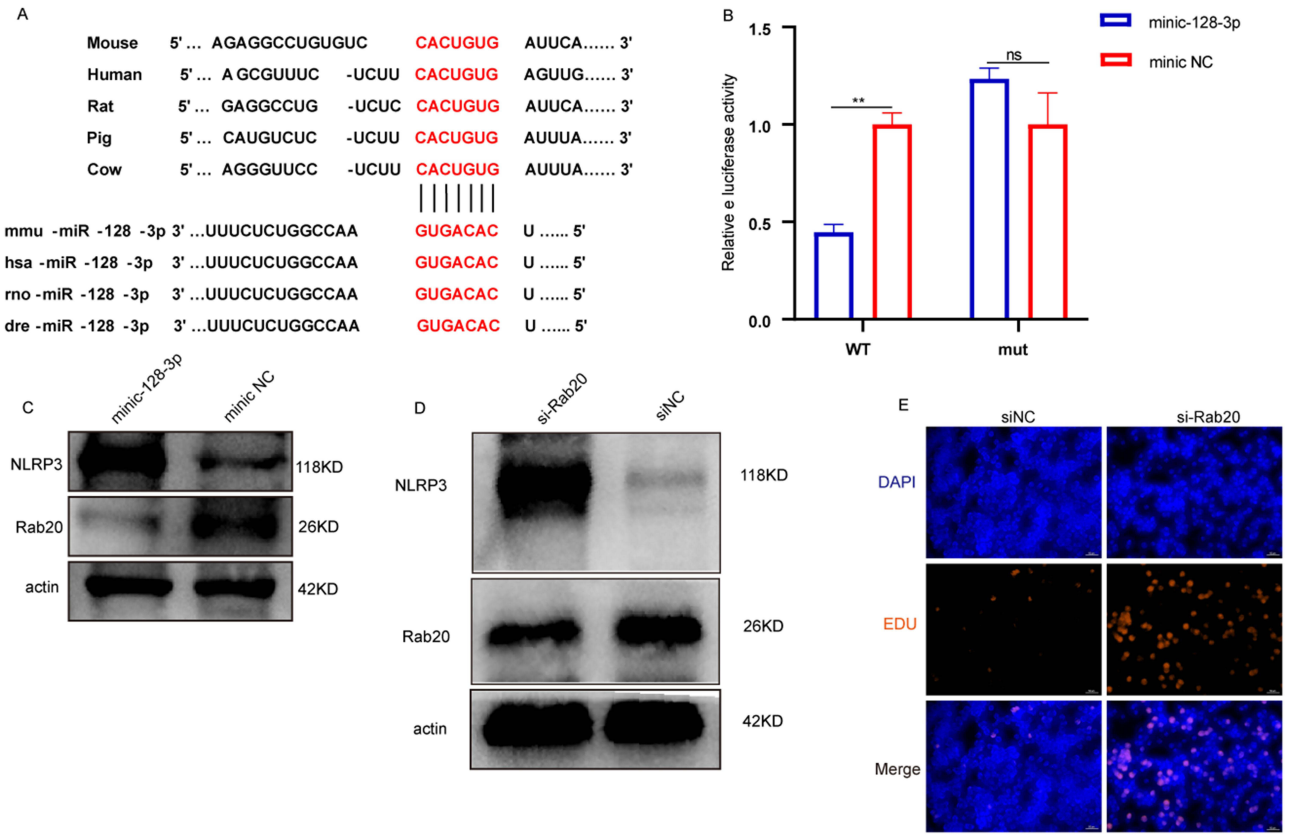

Figure 7 miR-128-3p enhances macrophage proliferation and inflammation by targeting Rab20. (**A**) Conservation of the target site for miR-128-3p within the 3' UTR of Rab20 across different species, along with the conservation of the miR-128-3p sequence itself in various species. (**B**) A dual luciferase reporter assay was conducted in 293T cells, where cells were co-transfected with wild-type or mutant Rab20 3' UTR luciferase reporter plasmids alongside minic-miR-128-3p or minic-miR-128-3p NC, followed by incubation with a renin-active substrate. Firefly luciferase activity was quantified as an indicator of overall luciferase activity (n=6). (**C**) Protein levels of Rab20 and NLRP3 were assessed via Western blotting following incubation with engineered exosomes containing minic-miR-128-3p and minic-miR-128-3p NC; β-actin served as an internal control. (**D**) Following transfection with siRab20, protein levels of Rab20 and NLRP3 were measured through Western blot analysis, utilizing β-actin as an internal control. (**E**) The impact of lung-derived exosomes on macrophage proliferation was determined using the EDU assay post-transfection with siRab20 (n=6), scale bar 50μm. $^{**}P<0.01$, ns $P>0.05$.

Furthermore, we assessed the impact of lung Ti-EVs on Rab20 expression within macrophages. Silencing Rab20 resulted in increased NLRP3 levels and promoted macrophage proliferation (Figure 7D and E).

Discussion

A growing body of research underscores the pivotal role of inflammation in lung injury and repair processes. Concurrently, macrophage heterogeneity—typically characterized by M1 and M2 states—is recognized as a complex and nuanced phenomenon that is significantly influenced by microenvironmental signals, including EVs.[31] This study presents, for the first time, an analysis of the types and expression profiles of miRNAs within lung Ti-EVs sourced from lung tissue in sepsis-related ALI. Furthermore, it elucidates how miR-128-3p contained in these Ti-EVs targets Rab20 to activate the NLRP3 signaling pathway, thereby promoting M1 polarization of macrophages and exacerbating the pathological progression of ALI.

In this experimental study, we successfully isolated tissue-derived Ti-EVs from lung tissues of sepsis-induced ALI mice for the first time. We induced ALI in mice using the well-established CLP model, followed by extraction of Ti-EVs from the lung tissues of these sepsis-induced ALI mice. Characterization confirmed that the isolated vesicles were indeed tissue-derived rather than cell-derived extracellular vesicles. To investigate whether lung Ti-EVs contribute to lung injury, we labeled these EVs with DiR dye and administered them to mice via intratracheal injection. In vivo imaging revealed that the labeled Ti-EVs accumulated within the pulmonary parenchyma. Notably, this observation aligns with previous reports confirming that lung Ti-EVs can localize to the pulmonary parenchyma.[23] Subsequently, we injected Ti-EVs derived from septic ALI lung tissue into normal mice through intratracheal administration. Our findings demonstrated that histological analysis via HE staining

https://doi.org/10.2147/IJN.S510241

indicated pathological changes; qRT-PCR revealed elevated levels of inflammatory cytokines IL-1β, IL-6, and TNF-α; and immunofluorescence assays showed alterations in macrophage numbers and polarization fluorescence intensity—all suggesting that lung Ti-EVs sourced from septic ALI lungs are capable of inducing acute lung injury. In a similar context, research conducted by Cecilia Lasser et al demonstrated that lung Ti-EVs are implicated in various pulmonary inflammatory diseases.[24] However, following intraperitoneal administration of GW4869, an exosome inhibitor, to mice—intended to suppress the production and release of Ti-EVs derived from ALI lung tissue—we observed that GW4869 effectively inhibited the generation of these Ti-EVs. This was substantiated through histological analysis revealing pathological changes, qRT-PCR quantifying levels of inflammatory cytokines IL-1β, IL-6, and TNF-α, as well as immunofluorescence assays assessing alterations in macrophage numbers and polarization fluorescence intensity. Xinyu Ge et al demonstrated that ischemia-reperfusion (IR) induces an increase in the release of EVs from the heart, termed IR-EVs, and that the transfer of these IR-EVs exacerbates cardiac damage associated with IR. GW4869 effectively inhibits both the production and release of EVs, thereby mitigating IR-induced injury.[32] Our research findings are consistent with those reported in the literature cited below. Xiaofeng Qin et al reported that pretreatment with exosome inhibitor GW4869 can alleviate pulmonary fibrosis as well as reduce levels of TNF-α, IL-1β, and IL-6 in bronchoalveolar lavage fluid.[33] Yang Shao et al indicated that GW4869 suppresses NLRP3 inflammasome-mediated necroptosis in intestinal cells and alleviates intestinal barrier damage during severe acute pancreatitis. Moreover, inflammatory responses and distant organ injuries—specifically to the kidneys and lungs—associated with severe acute pancreatitis were improved following GW4869 treatment.[34] Therefore, timely inhibition of harmful EVs production and release represents a promising strategy for treating ALI.

Although EVs encompass a diverse array of bioactive molecules, studies have demonstrated that their biological effects on target cells are partially contingent upon the content of the loaded miRNAs. Exosomal miRNAs have emerged as novel regulators of cellular functions, playing pivotal roles in the pathogenesis of cancer and inflammatory diseases. Chao Wang et al reported that levels of miR-155 in serum EVs from smokers were significantly elevated and correlated with carotid plaque formation as assessed by ultrasound imaging.[35] Rares Drula et al found that physiological concentrations of 17β-estradiol inhibit miR-149-5p, thereby obstructing its regulatory activity towards SP1 and specifically enhancing the secretion of EVs from estrogen receptor-positive breast cancer cells.[36] Yu Ning et al indicated that silencing miR-139-3p in MSCATV-EVs derived from atorvastatin-pretreated bone marrow mesenchymal stem cells markedly diminished this effect, while overexpression of miR-139-3p in mesenchymal stem cell-derived EVs augmented M2 polarization through inhibition of downstream signal transducer and activator of transcription 1.[37] Therefore, based on additional experimental studies alongside our sequencing results, we identified a set of inflammation-related miRNAs present in lung Ti-EVs: miR-128-3p, miR-196b-5p, miR-196a-5p, miR-130b-5p, miR-5099, miR-18b-5p, miR-215–5p, and miR1946a.

Our study revealed that lung Ti-EVs derived from sepsis-induced ALI mice exhibited differentially expressed miRNAs. While the expression levels of miRNAs such as miR-196b-5p, miR-196a-5p, and miR-1946a were also upregulated in these EVs, the most significant increase was observed for miR-128-3p. This finding suggests that miR-128-3p may play a critical role in modulating the inflammatory activity of exosomes. Indeed, as a highly conserved and pivotal miRNA, the involvement of miR-128-3p has been extensively studied in various conditions including esophageal squamous cell carcinoma, lung cancer, and renal inflammation.[38–40] Liuzhong Wu et al demonstrated that miR-128-3p expression was significantly upregulated following TNF-α stimulation. The overexpression of miR-128-3p exacerbated the inflammatory response induced by TNF-α, whereas inhibition of miR-128-3p effectively mitigated the inflammatory response in bone marrow mesenchymal stem cells.[41] Lin Wang et al reported that in LPS-induced septic acute kidney injury, miR-128-3p targets NRP1 to promote infiltration of inflammatory cells, enhance the expression of inflammatory factors, decrease renal cell viability, and increase apoptosis.[42] Haibo Xie et al found a dramatic increase in miR-128-3p expression in CLP or LPS-induced sepsis animal models; additionally, overexpression of miR-128-3p facilitated lung epithelial cell damage and macrophage inflammation.[43]

Our study reveals that lung tissue-derived Ti-EVs exacerbate sepsis-induced ALI by promoting inflammatory responses and macrophage polarization. In vivo experiments demonstrated that intratracheal administration of lung tissue-derived Ti-EVs in mice significantly elevated proinflammatory cytokines (TNF-α, IL-1β, and IL-6), aggravated histopathological damage, increased macrophage infiltration, and enhanced M1 macrophage activation. To establish the causal role of Ti-EVs miR-128-3p in ALI progression, engineered EVs carrying agomir-miR-128-3p were administered intratracheally, resulting in markedly amplified inflammatory cytokine expression, intensified histopathological

alterations (as evidenced by HE staining), substantial macrophage accumulation, and pronounced M1 macrophage polarization. Further mechanistic investigations revealed that in vitro co-culture of macrophages with engineered exosomes containing mimic-miR-128-3p upregulated NLRP3 protein expression while downregulating Rab20, concomitant with enhanced inflammatory cytokine production, accelerated macrophage proliferation, and preferential M1 phenotype differentiation. Collectively, these findings indicate that lung tissue-derived Ti-EVs miR-128-3p aggravates ALI through modulation of the Rab20-NLRP3 signaling axis.

MiRNAs are believed to regulate numerous complex physiological processes by inhibiting the expression of target genes with related functions.[44] Through a database search, we identified Rab20 as a potential target of miR-128-3p. Rab20 is a member of the Rab GTPase family that regulates the membrane transport of phagolysosomal vesicles by controlling EVs selection, vesicle generation, movement, connection, and fusion; it plays a crucial role in the innate immune response against pathogens.[45–47] Studies have shown that reduced levels of Rab20 in monocytes and macrophages are closely associated with the development of silicosis in miners. Furthermore, deficiency in Rab20 promotes activation of the NLRP3 inflammasome induced by silica crystals, thereby facilitating lung interstitial fibrosis and impairing respiratory function.[48] Research indicates that RAB20 serves as a biomarker for interstitial lung disease associated with connective tissue disorders found in bronchoalveolar lavage fluid.[49] Our experimental investigations demonstrated that co-culture of macrophages with lung tissue-derived extracellular vesicles containing miR-128-3p resulted in suppressed Rab20 protein expression and elevated inflammatory mediator levels. Notably, exogenous supplementation of miR-128-3p-overexpressing extracellular vesicles exacerbated these effects, showing more pronounced Rab20 suppression and intensified inflammatory responses, consistent with previous reports in this research field.

Drawing from existing literature, we identified Rab20 as a downstream target of NLRP3.[48] NLRP3 serves as a crucial sensor in the innate immune system, detecting exogenous pathogen invasion and endogenous cellular damage, and responding by forming a supramolecular complex known as the NLRP3 inflammasome to activate cysteine-aspartate protease-1.[50] Wen-Jing Zhong et al demonstrated that inhibition of glycolysis using 2-deoxyglucose can diminish the activation of the NLRP3 inflammasome in macrophages triggered by myeloid cell receptor-1.[51] Xiaoyang Wu et al reported that HO-1 regulates macrophage polarization via the TXNIP/NLRP3 signaling pathway.[52] Haijin Lv et al indicated that negatively regulating NLRP3 inflammasome activation in alveolar macrophages can ameliorate pathological changes and lung injury-related indicators in ALI models while reducing pro-inflammatory cytokine levels, thereby modulating M1/M2 macrophage balance.[53] Our experimental data demonstrated that co-culture of macrophages with lung tissue-derived extracellular vesicles containing miR-128-3p led to upregulated NLRP3 protein expression and elevated inflammatory mediator levels. Furthermore, exogenous supplementation of miR-128-3p-overexpressing extracellular vesicles resulted in more pronounced NLRP3 upregulation and significantly amplified proinflammatory responses TNF-α, IL-1β, and IL-6). Intriguingly, siRNA-mediated silencing of Rab20 similarly induced NLRP3 protein overexpression, consistent with previous mechanistic studies investigating the Rab20-NLRP3 regulatory axis in macrophage activation.

EVs carry a variety of molecules involved in intercellular communication and have garnered significant attention for their potential as drug delivery systems.[54] Several engineering approaches have been explored for the loading of these vesicles. In this study, we investigated the nucleic acid loading of miR-128-3p agonists or inhibitors onto EVs isolated from lung tissue via electroporation. First, we assessed the effects of voltage and pulse duration on vesicle morphology, loading capacity, and miRNA transfer to target cells. Second, mild electroporation proved to be more effective and provided superior protection for miRNA against RNase degradation compared to direct incubation with EVs. Furthermore, electroporation preserved the original contents of the vesicles—including RNAs and proteins—and maintained their uptake capability by target cells, indicating that the integrity of the vesicles was not compromised during this process. Our findings demonstrate that lung tissue-derived EVs can be effectively and functionally loaded with miRNA using an electroporation method that maintains their structural integrity. Finally, this study also has certain limitations, as the origin of exosomes from pulmonary tissue was not tracked.

In summary, our study demonstrates the presence of abundant pulmonary alveolar exosomes in mice with ALI, which are specifically loaded with miRNAs, including miR-128-3p. In vivo experiments indicate that these pulmonary alveolar exosomes can effectively reach pulmonary macrophages and induce lung injury. Furthermore, in vitro studies reveal that miR-128-3p derived from pulmonary alveolar exosomes promotes macrophage proliferation and inflammation by

targeting Rab20. This research underscores the significance of pulmonary alveolar exosomes in modulating the activation process of macrophages. This novel intercellular communication pathway may enhance our understanding of ALI mechanisms following exposure to various stimuli, such as sepsis.

Conclusions

Ti-EVs miR-128-3p derived from lung tissue in sepsis-induced ALI activates the NLRP3 signaling pathway by targeting Rab20, leading to M1 polarization of macrophages and aggravating ALI. This study reveals the importance of extracellular vesicles derived from lung tissue in regulating macrophage activation during sepsis. This novel intercellular communication pathway may help to better understand the mechanism of ALI after exposure to various stimuli (such as sepsis). In the future, it is necessary to further explore whether the level of miR-128-3p in Ti-EVs derived from lung tissue can serve as a prognostic biomarker for the progression of ALI in patients with sepsis.

Data Sharing Statement

The data that support the findings of this study are available from the corresponding author, Fen Liu, upon reasonable request.

Ethics Approval

All animal experiments received approval from the Animal Ethics Committee of the First Affiliated Hospital of Nanchang University (Ethics Approval Number: CDYFY-IACUC-202302QR051) and were conducted in compliance with the National Institutes of Health (NIH) guidelines for the care and use of laboratory animals, as well as relevant regulations outlined in China's Regulations on the Administration of Experimental Animals.

Additional Information

I hereby confirm that this submission has not been considered or reviewed by any other journal prior to this submission.

Acknowledgments

This work was supported by grants from the Natural Science Foundation of China (No. 81660315), ChinaJiangxi Province Nature Fund project (No.20242BAB20386 and 20232ACB206046) and Young Scholar Project of the First Affiliated Hospital of Nanchang University (No.YFYPY202428).

Author Contributions

All authors contributed significantly to the reported work, encompassing aspects such as conception, study design, execution, data acquisition, analysis and interpretation. They participated in drafting, revising, or critically reviewing the manuscript; provided final approval for the version intended for publication; agreed on the journal selected for submission; and accept responsibility for all facets of the work.

Disclosure

The authors declare that this study was conducted free from any commercial or financial relationships that could be perceived as a potential conflict of interest.

References

1. Xie J, Wang H, Kang Y. et al. The epidemiology of sepsis in Chinese ICUs: a National Cross-Sectional Survey. *Crit Care Med*. 2020;48(3):e209–e218. doi:10.1097/CCM.0000000000004155
2. Bruno RR, Wernly B, Mamandipoor B, et al. ICU-mortality in old and very old patients suffering from sepsis and septic shock. *Front Med Lausanne*. 2021;8:697884. doi:10.3389/fmed.2021.697884
3. Wiersinga WJ, van der Poll T. Immunopathophysiology of human sepsis. *EBioMedicine*. 2022;86:104363. doi:10.1016/j.ebiom.2022.104363
4. Sevransky JE, Martin GS, Shanholtz C, et al. Mortality in sepsis versus non-sepsis induced acute lung injury. *Crit Care*. 2009;13(5):R150. doi:10.1186/cc8048
5. Bellani G, Laffey JG, Pham T, et al. Epidemiology, patterns of care, and mortality for patients with acute respiratory distress syndrome in intensive care units in 50 countries. *JAMA*. 2016;315(8):788–800. doi:10.1001/jama.2016.0291

6. Nanchal RS, Truwit JD, Bollag L. Recent advances in understanding and treating acute respiratory distress syndrome. *F1000Res*. 2018;7:7. doi:10.12688/f1000research.13350.2
7. Wang Z, Wang Z. The role of macrophages polarization in sepsis-induced acute lung injury. *Front Immunol*. 2023;14:1209438. doi:10.3389/fimmu.2023.1209438
8. Yunna C, Mengru H, Lei W, Weidong C. Macrophage M1/M2 polarization. *Eur J Pharmacol*. 2020;877:173090. doi:10.1016/j.ejphar.2020.173090
9. Courties G, Heidt T, Sebas M, et al. In vivo silencing of the transcription factor IRF5 reprograms the macrophage phenotype and improves infarct healing. *J Am Coll Cardiol*. 2014;63(15):1556–1566. doi:10.1016/j.jacc.2013.11.023
10. Cheng P, Li S, Chen H. Macrophages in lung injury, repair, and fibrosis. *Cells*. 2021;10(2):436. doi:10.3390/cells10020436
11. Gunassekaran GR, Poongkavithai Vadevoo SM, Baek MC, Lee B. M1 macrophage exosomes engineered to foster M1 polarization and target the IL-4 receptor inhibit tumor growth by reprogramming tumor-associated macrophages into M1-like macrophages. *Biomaterials*. 2021;278:121137. doi:10.1016/j.biomaterials.2021.121137
12. Yang J, Huang X, Yu Q, et al. Extracellular vesicles derived from M2-like macrophages alleviate acute lung injury in a miR-709-mediated manner. *J Extracell Vesicles*. 2024;13(4):e12437. doi:10.1002/jev2.12437
13. Pegtel DM, Gould SJ. Exosomes. *Annu Rev Biochem*. 2019;88(1):487–514. doi:10.1146/annurev-biochem-013118-111902
14. Krylova SV, Feng D. The machinery of exosomes: biogenesis, release, and uptake. *Int J mol Sci*. 2023;24(2):1337. doi:10.3390/ijms24021337
15. Deng W, Lu Y, Hu P, et al. Integrated analysis of non-coding RNA and mRNA expression profiles in exosomes from lung tissue with sepsis-induced acute lung injury. *J Inflamm Res*. 2023;16:3879–3895. doi:10.2147/JIR.S419491
16. Han QF, Li WJ, Hu KS, et al. Exosome biogenesis: machinery, regulation, and therapeutic implications in cancer. *mol Cancer*. 2022;21(1):207. doi:10.1186/s12943-022-01671-0
17. Mori MA, Ludwig RG, Garcia-Martin R, Brandao BB, Kahn CR. Extracellular miRNAs: from biomarkers to mediators of physiology and disease. *Cell Metab*. 2019;30(4):656–673. doi:10.1016/j.cmet.2019.07.011
18. Xiong C, Huang X, Chen S, Li Y. Role of extracellular microRNAs in sepsis-induced acute lung injury. *J Immunol Res*. 2023;2023:5509652. doi:10.1155/2023/5509652
19. Hu Q, Zhang S, Yang Y, et al. Extracellular vesicles in the pathogenesis and treatment of acute lung injury. *Mil Med Res*. 2022;9(1):61. doi:10.1186/s40779-022-00417-9
20. Breglio AM, May LA, Barzik M, et al. Exosomes mediate sensory hair cell protection in the inner ear. *J Clin Invest*. 2020;130(5):2657–2672. doi:10.1172/JCI128867
21. Penas-Martinez J, Barrachina MN, Cuenca-Zamora EJ, et al. Qualitative and quantitative comparison of plasma exosomes from neonates and adults. *Int J mol Sci*. 2021;22(4):1926. doi:10.3390/ijms22041926
22. Camino T, Lago-Baameiro N, Bravo SB, et al. Vesicles shed by pathological murine adipocytes spread pathology: characterization and functional role of insulin resistant/hypertrophied adiposomes. *Int J mol Sci*. 2020;21(6):2252. doi:10.3390/ijms21062252
23. Liu B, Jin Y, Yang J, et al. Extracellular vesicles from lung tissue drive bone marrow neutrophil recruitment in inflammation. *J Extracell Vesicles*. 2022;11(5):e12223. doi:10.1002/jev2.12223
24. Lasser C, Kishino Y, Park KS, et al. Immune-associated proteins are enriched in lung tissue-derived extracellular vesicles during allergen-induced eosinophilic airway inflammation. *Int J mol Sci*. 2021;22(9):4718. doi:10.3390/ijms22094718
25. Chen SY, Chen YL, Li PC, et al. Engineered extracellular vesicles carrying let-7a-5p for alleviating inflammation in acute lung injury. *J Biomed Sci*. 2024;31(1):30. doi:10.1186/s12929-024-01019-4
26. Rittirsch D, Huber-Lang MS, Flierl MA, Ward PA. Immunodesign of experimental sepsis by cecal ligation and puncture. *Nat Protoc*. 2009;4(1):31–36. doi:10.1038/nprot.2008.214
27. Tang X, Ren H, Guo M, Qian J, Yang Y, Gu C. Review on circular RNAs and new insights into their roles in cancer. *Comput Struct Biotechnol J*. 2021;19:910–928. doi:10.1016/j.csbj.2021.01.018
28. Vella LJ, Scicluna BJ, Cheng L, et al. A rigorous method to enrich for exosomes from brain tissue. *J Extracell Vesicles*. 2017;6(1):1348885. doi:10.1080/20013078.2017.1348885
29. Wang G, Jin S, Huang W, et al. LPS-induced macrophage HMGB1-loaded extracellular vesicles trigger hepatocyte pyroptosis by activating the NLRP3 inflammasome. *Cell Death Discov*. 2021;7(1):337. doi:10.1038/s41420-021-00729-0
30. Catalano M, O'Driscoll L. O'Driscoll L: inhibiting extracellular vesicles formation and release: a review of EV inhibitors. *J Extracell Vesicles*. 2020;9(1):1703244. doi:10.1080/20013078.2019.1703244
31. Ismail N, Wang Y, Dakhlallah D, et al. Macrophage microvesicles induce macrophage differentiation and miR-223 transfer. *Blood*. 2013;121(6):984–995. doi:10.1182/blood-2011-08-374793
32. Ge X, Meng Q, Wei L, et al. Myocardial ischemia-reperfusion induced cardiac extracellular vesicles harbour proinflammatory features and aggravate heart injury. *J Extracell Vesicles*. 2021;10(4):e12072. doi:10.1002/jev2.12072
33. Qin X, Lin X, Liu L, et al. Macrophage-derived exosomes mediate silica-induced pulmonary fibrosis by activating fibroblast in an endoplasmic reticulum stress-dependent manner. *J Cell mol Med*. 2021;25(9):4466–4477. doi:10.1111/jcmm.16524
34. Shao Y, Jiang Y, Wang J, Li H, Li C, Zhang D. Inhibition of circulating exosomes release with GW4869 mitigates severe acute pancreatitis-stimulated intestinal barrier damage through suppressing NLRP3 inflammasome-mediated pyroptosis. *Int Immunopharmacol*. 2024;126:111301. doi:10.1016/j.intimp.2023.111301
35. Wang C, Liu C, Shi J, et al. Nicotine exacerbates endothelial dysfunction and drives atherosclerosis via extracellular vesicle-miRNA. *Cardiovasc Res*. 2023;119(3):729–742. doi:10.1093/cvr/cvac140
36. Drula R, Pardini B, Fu X, et al. 17beta-estradiol promotes extracellular vesicle release and selective miRNA loading in ERalpha-positive breast cancer. *Proc Natl Acad Sci U S A*. 2023;120(23):e2122053120. doi:10.1073/pnas.2122053120
37. Ning Y, Huang P, Chen G, et al. Atorvastatin-pretreated mesenchymal stem cell-derived extracellular vesicles promote cardiac repair after myocardial infarction via shifting macrophage polarization by targeting microRNA-139-3p/Stat1 pathway. *BMC Med*. 2023;21(1):96. doi:10.1186/s12916-023-02778-x
38. Zhao L, Li R, Xu S, et al. Tumor suppressor miR-128-3p inhibits metastasis and epithelial-mesenchymal transition by targeting ZEB1 in esophageal squamous-cell cancer. *Acta Biochim Biophys Sin (Shanghai)*. 2018;50(2):171–180. doi:10.1093/abbs/gmx132

39. Koh H, Park H, Chandimali N, et al. MicroRNA-128 suppresses paclitaxel-resistant lung cancer by inhibiting MUC1-C and BMI-1 in cancer stem cells. *Oncotarget*. 2017;8(66):110540–110551. doi:10.18632/oncotarget.22818
40. Shyamasundar S, Ong C, Yung LL, Dheen ST, Bay BH. miR-128 regulates genes associated with inflammation and fibrosis of rat kidney cells in vitro. *Anat Rec (Hoboken)*. 2018;301(5):913–921. doi:10.1002/ar.23763
41. Wu L, Zhang G, Guo C, Zhao X, Shen D, Yang N. MiR-128-3p mediates TNF-alpha-induced inflammatory responses by regulating Sirt1 expression in bone marrow mesenchymal stem cells. *Biochem Biophys Res Commun*. 2020;521(1):98–105. doi:10.1016/j.bbrc.2019.10.083
42. Wang L, Wang K, Tian Z. Tian Z: miR-128-3p Inhibits NRP1 expression and promotes inflammatory response to acute kidney injury in sepsis. *Inflammation*. 2020;43(5):1772–1779. doi:10.1007/s10753-020-01251-8
43. Xie H, Chai H, Du X, Cui R, Dong Y. Overexpressing long non-coding RNA OIP5-AS1 ameliorates sepsis-induced lung injury in a rat model via regulating the miR-128-3p/Sirtuin-1 pathway. *Bioengineered*. 2021;12(2):9723–9738. doi:10.1080/21655979.2021.1987132
44. Nowek K, Sun SM, Bullinger L, et al. Aberrant expression of miR-9/9* in myeloid progenitors inhibits neutrophil differentiation by post-transcriptional regulation of ERG. *Leukemia*. 2016;30(1):229–237. doi:10.1038/leu.2015.183
45. Egami Y, Araki N. Rab20 regulates phagosome maturation in RAW264 macrophages during Fc gamma receptor-mediated phagocytosis. *PLoS One*. 2012;7(4):e35663. doi:10.1371/journal.pone.0035663
46. Zhao S, Xi D, Cai J, et al. Rab20 is critical for bacterial lipoprotein tolerization-enhanced bactericidal activity in macrophages during bacterial infection. *Sci China Life Sci*. 2020;63(3):401–409. doi:10.1007/s11427-019-9527-3
47. Liu BHM, Tey SK, Mao X, et al. TPI1-reduced extracellular vesicles mediated by Rab20 downregulation promotes aerobic glycolysis to drive hepatocarcinogenesis. *J Extracell Vesicles*. 2021;10(10):e12135. doi:10.1002/jev2.12135
48. Peng Z, Duan M, Zhao K, Tang Y, Liang F. RAB20 deficiency promotes the development of silicosis via NLRP3 inflammasome. *Front Immunol*. 2022;13:967299. doi:10.3389/fimmu.2022.967299
49. Ye J, Liu P, Li R, et al. Biomarkers of connective tissue disease-associated interstitial lung disease in bronchoalveolar lavage fluid: a label-free mass spectrometry-based relative quantification study. *J Clin Lab Anal*. 2022;36(5):e24367. doi:10.1002/jcla.24367
50. Fu J, Wu H. Structural Mechanisms of NLRP3 Inflammasome Assembly and Activation. *Annu Rev Immunol*. 2023;41(1):301–316. doi:10.1146/annurev-immunol-081022-021207
51. Zhong WJ, Liu T, Yang HH, et al. TREM-1 governs NLRP3 inflammasome activation of macrophages by firing up glycolysis in acute lung injury. *Int J Biol Sci*. 2023;19(1):242–257. doi:10.7150/ijbs.77304
52. Wu X, Wu L, Wu Y, et al. Heme oxygenase-1 ameliorates endotoxin-induced acute lung injury by modulating macrophage polarization via inhibiting TXNIP/NLRP3 inflammasome activation. *Free Radic Biol Med*. 2023;194:12–22. doi:10.1016/j.freeradbiomed.2022.11.032
53. Lv H, Yuan X, Zhang J, et al. Heat shock preconditioning mesenchymal stem cells attenuate acute lung injury via reducing NLRP3 inflammasome activation in macrophages. *Stem Cell Res Ther*. 2021;12(1):290. doi:10.1186/s13287-021-02328-3
54. Cecchin R, Troyer Z, Witwer K, Morris KV. Extracellular vesicles: the next generation in gene therapy delivery. *mol Ther*. 2023;31(5):1225–1230. doi:10.1016/j.ymthe.2023.01.021